



# Verification of strain gradient elasticity computation by analytical solutions

Hua Yang<sup>1</sup>  | Dmitry Timofeev<sup>2</sup> | B. Emek Abali<sup>3</sup>  | Baotong Li<sup>4</sup> | Wolfgang H. Müller<sup>1</sup>

<sup>1</sup> Technische Universität Berlin, Berlin, Germany

<sup>2</sup> Università degli Studi dell'Aquila, L'Aquila, Italy

<sup>3</sup> Uppsala University, Uppsala, Sweden

<sup>4</sup> Xi'an Jiaotong University, Xi'an, China

## Correspondence

Hua Yang, Technische Universität Berlin, Berlin, Germany.

Email: [hua.yang@campus.tu-berlin.de](mailto:hua.yang@campus.tu-berlin.de)

As there are different computational methods for simulating problems in generalized mechanics, we present simple applications and their closed-form solutions for verifying a numerical implementation. For such a benchmark, we utilize these analytical solutions and examine three-dimensional numerical simulations by the finite element method (FEM) using IsoGeometric Analysis (IGA) with the aid of open source codes, called tIGAr, developed within the FEniCS platform. A study for the so-called wedge forces and double tractions help to comprehend their roles in the displacement solution as well as examine the significance by comparing to the closed form solutions for given boundary conditions. It is found that numerical results are in a good agreement with the analytical solutions if wedge forces and double tractions are considered. It is also presented how the wedge forces become necessary in order to maintain equilibrium in strain gradient materials.

## KEYWORDS

analytical solutions, strain gradient elasticity, three-dimensional problems

## 1 | INTRODUCTION

Miniaturization of sensors and actuators, such as micro-electro mechanical systems (MEMS), necessitates an accurate modeling of materials at micrometer length scale (microscale). However, from experimental evidences [61] one can observe stiffening or softening material responses at the microscale when compared to a solution based on the Cauchy–Boltzmann continuum, that is, conventional elasticity theory. In order to capture these geometric length dependent phenomena, which are commonly referred to as size effects, a generalization of standard elasticity theory is required, such that the stored energy depends not only on strain but also on other primitive variables, for example, the spin or the strain gradient [5, 16, 37, 62]. Various theories of such a generalized mechanics are described in the literature. They are mathematically close and may be considered as particular cases of a unified theory [64]. For historical and philosophical remarks on the subject, we refer to [27, 29].

In the so-called strain gradient elasticity theory the stored energy is considered to be dependent on strains as well as strain gradients. Motivation for introducing higher order gradient of strains in the stored energy arises from various aspects, we refer to [1, 7, 11, 31, 36, 63, 86]. First, an investigation of highly localized phenomena, such as crack

This is an open access article under the terms of the [Creative Commons Attribution](https://creativecommons.org/licenses/by/4.0/) License, which permits use, distribution and reproduction in any medium, provided the original work is properly cited.

© 2021 The Authors. *ZAMM - Journal of Applied Mathematics and Mechanics* published by Wiley-VCH GmbH.

formation and propagation, may be realized by involving higher order gradients in order to regularize the solution of cracks by penalizing the displacements, which are localized above a given threshold [17, 68, 71, 73, 78, 93]. Second, an accurate modeling of metamaterials is achieved in the framework of strain gradient theory [16, 26, 28, 35, 38, 40, 45, 89]. Indeed, the behaviors of metamaterials depend on the morphology of microstructures [23, 43, 53, 54] and show peculiar behaviors, such as size effects [3, 90–92] and band gaps [76, 80], which are not captured by the classical Cauchy continuum. Exotic material behaviors may be governed by internal or boundary layers of higher strain gradients [51]. As an example of metamaterials we refer to materials with pantographic substructures [32, 34] having non-negligible strain gradient terms in the formulation of deformation energy [24,25,41,65,88], which are found in recent numerical and experimental evidences, for example, in shearing tests [15], three-point bending tests [94], compression tests [87], or torsion tests [60]. A homogenization procedure of pantographic microstructures leading to second gradient materials is shown in [12–14, 84]. Generally speaking, generalized mechanics at the macroscale results in as a homogenization procedure from the Cauchy–Boltzmann continuum at the micrometer length-scale (microscale) [57]. Strain gradient theory is able to sustain the so-called wedge forces [9, 56, 77], which are acting on corners (point forces) in 2D and edges (force distributions along lines) in 3D, while the classical Cauchy continuum leads to singularities when handling such issues. From [8, 33, 48, 83], it becomes obvious that the reasons of inducing higher order strain gradient allows a continuum to sustain boundary conditions on vertices and edges of a body.

Strain gradient theory leads to higher order partial differential equations and requires an interpolation scheme for the finite element representation to guarantee a correspondingly higher order of continuity. For this reason, various numerical implementations of strain gradient theories are proposed in the literature, such as the mixed formulation [67, 85],  $C^1$  continuous elements [42, 66, 95], and isogeometric analysis [39, 56,81]. The concept of IGA [46] is a mesh-based numerical approach using shape functions in FEM identical as the basic functions in CAD generated from NURBS (Non-Uniform Rational B-Splines). In the context of strain gradient elasticity, such a formulation serves the  $C^n$  continuity across the element boundaries. The NURBS interpolation requires only displacements as nodal degrees of freedom, and no derivatives of the displacement field are needed [39]. Some examples can be found in [19–21, 82]. From a general viewpoint, for verification purposes, a numerical solution have to be compared to analytical results [79]. Some analytical derivations were presented for 2D cases [22, 69, 74, 75, 95]. Obtaining results of this kind for 3D cases is rather challenging.

In this paper, closed-form analytical solutions [70, 72, 74] are presented for cases of three dimensional benchmark problems for a centro-symmetric and isotropic material modeled by strain gradient theory. The balance equations and the boundary terms (tractions, double tractions, and wedge forces on the boundaries) are derived by means of the variational method. Numerical implementations have been developed based on IGA (Iso-Geometric Analysis) for these classical cases in order to demonstrate the benchmarking procedure. The aim of the paper is to verify our implementation based on an IGA library called tIGAr [49, 50] provided on the FEniCS platform. Moreover, a comparative study allows us to understand the roles of wedge forces in maintaining equilibrium. The code uses open-source packages under GNU public license [44], and we make the codes publicly available in [2] in order to enable a scientific exchange. The paper is organized as follows: The variational formulation of strain gradient elasticity theory [1, 30] is outlined in Section 2. The formulation of three-dimensional problem is shown in Section 3. In Section 4 analytical and numerical results are compared for three different benchmark examples.

## 2 | STRAIN GRADIENT ELASTICITY

### 2.1 | Variational formulation

In this section, strain gradient elasticity as in [58, 59] will be revisited. Conventional continuum mechanics theories assume that stress at a material point is a function of state variables, such as strain, at the same point. This local assumption is adequate when the wavelength of a deformation field is orders in magnitude greater than the dominant micro-structural material length scale. However, when these two length scales are comparable, an extension becomes necessary, herein we use the strain gradient theory. Unlike the classical elasticity, in strain gradient theory the stored energy density depends on the strain,  $\varepsilon_{ij}$ , and on the strain gradient,  $\eta_{ijk}$ :

$$\varepsilon_{ij} = \frac{u_{i,j} + u_{j,i}}{2}, \quad \eta_{ijk} = \varepsilon_{ij,k} = \frac{u_{i,jk} + u_{j,ik}}{2}. \quad (1)$$

Here  $\mathbf{u}$  denotes the displacement field and a comma means differentiation in space,  $\mathbf{X}$ , expressed in Cartesian coordinates,

$$u_{i,j} = \frac{\partial u_i}{\partial X_j}, \quad X_j \in \Omega \subset \mathbb{R}^3 \quad (2)$$

For strain gradient materials, the stored energy density,  $w$ , depends on the first and second gradients of the displacement field

$$w = w(\varepsilon_{ij}, \eta_{ijk}). \quad (3)$$

We compute the first variation of functional for the internal energy of the body  $W^{\text{int}}$ :

$$W^{\text{int}} = \int_{\Omega} w \, dV, \quad (4)$$

such that we have

$$\delta W^{\text{int}} = \int_{\Omega} \delta w \, dV = \int_{\Omega} \left( \frac{\partial w}{\partial u_{i,j}} \delta u_{i,j} + \frac{\partial w}{\partial u_{i,jk}} \delta u_{i,jk} \right) dV, \quad (5)$$

where the variation of displacement  $\delta u_i$  is the test function in the finite element method to be used in simulations. After applying integration by parts, for the details we refer to the Appendix, we obtain

$$\begin{aligned} & \int_{\Omega} \left( \frac{\partial w}{\partial u_{i,j}} \delta u_{i,j} + \frac{\partial w}{\partial u_{i,jk}} \delta u_{i,jk} \right) dV \\ &= \int_{\Omega} \left( -\frac{\partial w}{\partial u_{i,j}} + \left( \frac{\partial w}{\partial u_{i,jk}} \right)_{,k} \right)_{,j} \delta u_i \, dV + \int_{\partial\Omega} n_j \left( \frac{\partial w}{\partial u_{i,j}} - \left( \frac{\partial w}{\partial u_{i,jk}} \right)_{,k} \right) \delta u_i \, dA + \int_{\partial\Omega} n_k \frac{\partial w}{\partial u_{i,jk}} \delta u_{i,j} \, dA. \end{aligned} \quad (6)$$

In the third integral of the right hand side of the equation above, on the boundary surface, the gradient of test function  $\delta u_{i,j}$  can be decomposed into a gradient within and normal to the surface [10, 18, 47, 52]:

$$\delta u_{i,j} = D_j(\delta u_i) + n_j D(\delta u_i), \quad (7)$$

where the operators  $D$  and  $D_j$  read

$$D(\cdot) = n_k \frac{\partial(\cdot)}{\partial X_k}, \quad D_j(\cdot) = (\delta_{jk} - n_j n_k) \frac{\partial(\cdot)}{\partial X_k}, \quad (8)$$

and  $n_i$  is the unit surface normal vector. Considering Equation (7), the last integral in Equation (6) becomes

$$\int_{\partial\Omega} n_k \frac{\partial w}{\partial u_{i,jk}} \delta u_{i,j} \, dA = \int_{\partial\Omega} n_k \frac{\partial w}{\partial u_{i,jk}} D_j(\delta u_i) \, dA + \int_{\partial\Omega} n_k \frac{\partial w}{\partial u_{i,jk}} n_j D(\delta u_i) \, dA. \quad (9)$$

The boundary surface is assumed to be divisible into a finite number of smooth parts,  $\partial\Omega_m$ , each bounded by an edge,  $\partial\partial\Omega_m$ . Using Stokes' divergence theorem by following [18] on each smooth surface, the following equation is obtained [52]

$$\int_{\partial\Omega_m} D_j \left( n_k \frac{\partial w}{\partial u_{i,jk}} \delta u_i \right) dA = \int_{\partial\Omega_m} n_j n_k \frac{\partial w}{\partial u_{i,jk}} D_p(n_p) \delta u_i \, dA + \oint_{\partial\partial\Omega_m} \nu_j n_k \frac{\partial w}{\partial u_{i,jk}} \delta u_i \, dl, \quad (10)$$

where  $\nu_j$  is the unit tangent vector and belongs to the tangent space to  $\partial\Omega_m$ . According to the chain rule, we have

$$\int_{\partial\Omega} D_j \left( n_k \frac{\partial w}{\partial u_{i,jk}} \delta u_i \right) dA = \int_{\partial\Omega} D_j \left( n_k \frac{\partial w}{\partial u_{i,jk}} \right) \delta u_i \, dA + \int_{\partial\Omega} D_j(\delta u_i) \left( n_k \frac{\partial w}{\partial u_{i,jk}} \right) dA. \quad (11)$$

Then the first integral on the right hand side of Equation (9) is written as

$$\int_{\partial\Omega} n_k \frac{\partial w}{\partial u_{i,jk}} D_j(\delta u_i) dA = \int_{\partial\Omega} n_i n_k \frac{\partial w}{\partial u_{i,jk}} (D_p n_p) \delta u_i dA + \sum_m \oint_{\partial\partial\Omega_m} \Delta \left( v_j n_k \frac{\partial w}{\partial u_{i,jk}} \right) \delta u_i dl - \int_{\partial\Omega} D_j \left( n_k \frac{\partial w}{\partial u_{i,jk}} \right) \delta u_i dA. \quad (12)$$

By  $\Delta(\cdot)$ , we denote the difference between values of the expression in the parentheses, which are calculated at different sides of a sharp edge. Note that integration domain of the third integral in Equation (10) is the boundary of a smooth surface. The whole body is composed of several smooth surfaces. By  $\sum_m$ , the sharp edges of the body are summed up. We stress that every edge line enters twice since it belongs to two adjacent surface regions [18]. By inserting the latter into Equation (11), the last surface integral in Equation (6) becomes

$$\begin{aligned} \int_{\partial\Omega} n_k \frac{\partial w}{\partial u_{i,jk}} \delta u_{i,j} dA &= \int_{\partial\Omega} n_i n_j \frac{\partial w}{\partial u_{i,jk}} (D_p n_p) \delta u_i dA + \sum_m \oint_{\partial\partial\Omega_m} \Delta \left( v_j n_k \frac{\partial w}{\partial u_{i,jk}} \right) \delta u_i dl \\ &\quad - \int_{\partial\Omega} D_j \left( n_k \frac{\partial w}{\partial u_{i,jk}} \right) \delta u_i dA + \int_{\partial\Omega} n_k \frac{\partial w}{\partial u_{i,jk}} n_j D \delta u_i dA. \end{aligned} \quad (13)$$

Thus the final integral form reads

$$\begin{aligned} \int_{\Omega} \delta w dV &= \int_{\Omega} \left( \frac{\partial w}{\partial u_{i,j}} \delta u_{i,j} + \frac{\partial w}{\partial u_{i,jk}} \delta u_{i,jk} \right) dV = \int_{\Omega} \left( -\frac{\partial w}{\partial u_{i,j}} + \left( \frac{\partial w}{\partial u_{i,jk}} \right)_{,k} \right)_{,j} \delta u_i dV \\ &\quad + \int_{\partial\Omega} \left( n_j \left( \frac{\partial w}{\partial u_{i,j}} - \left( \frac{\partial w}{\partial u_{i,jk}} \right)_{,k} \right) + n_k n_j \frac{\partial w}{\partial u_{i,jk}} (D_p n_p) - D_j \left( n_k \frac{\partial w}{\partial u_{i,jk}} \right) \right) \delta u_i dA \\ &\quad + \int_{\partial\Omega} n_k \frac{\partial w}{\partial u_{i,jk}} n_j D(\delta u_i) dA + \sum_m \oint_{\partial\partial\Omega_m} \Delta \left( v_j n_k \frac{\partial w}{\partial u_{i,jk}} \right) \delta u_i dl. \end{aligned} \quad (14)$$

For a better analogy, we define stress and hyperstress as follows:

$$\sigma_{ij} = \frac{\partial w}{\partial u_{i,j}}, \quad \tau_{ijk} = \frac{\partial w}{\partial u_{i,jk}}. \quad (15)$$

It is observed from the last two integrals in Equation (14) that second gradient continua can sustain external surface double forces and sustain external line forces [10].

According to the principle of virtual work,

$$\delta W^{\text{int}} - \delta W^{\text{ext}} = 0, \quad (16)$$

$W^{\text{ext}}$  is the external work done on the body. It is assumed to have the form [10, 52]:

$$W^{\text{ext}} = \int_{\Omega} b_i u_i dV + \int_{\partial\Omega} (t_i u_i + r_i D(u_i)) dA + \sum_m \oint_{\partial\partial\Omega_m} f_i u_i dl. \quad (17)$$

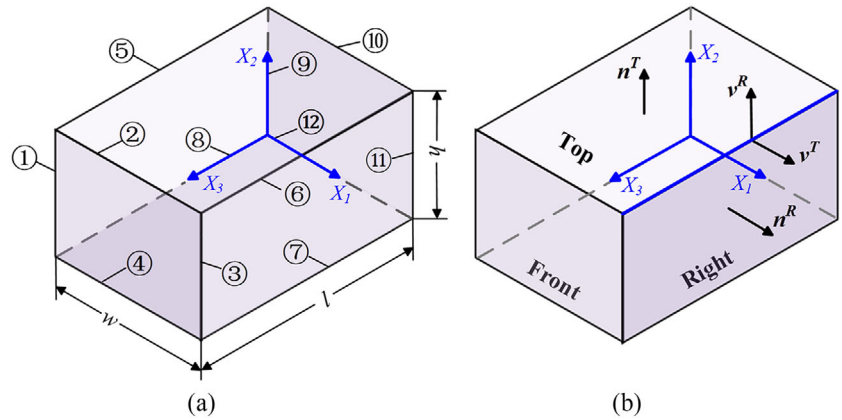
The first part,  $b_i u_i$ , is the energy density because of the specific force,  $b_i$  [4]. By Equations (14), (16), and (17), the so-called tractions  $t_i$ , double tractions  $r_i$  and wedge forces  $f_k$  are expressed as

$$\begin{aligned} t_i &= n_j (\sigma_{ij} - \tau_{ijk,k}) + n_k n_j \tau_{ijk} (D_p n_p) - D_j (n_k \tau_{ijk}), \\ r_i &= n_j n_k \tau_{ijk}, \\ f_i &= \Delta v_j n_k \tau_{ijk}. \end{aligned} \quad (18)$$

By inserting Equation (15), Equation (18) into Equation (16) with the aid of Equation (14), we find out the so-called governing equation:

$$(\sigma_{ij} - \tau_{ijk,k})_{,j} + b_i = 0. \quad (19)$$

**FIGURE 1** The schematic of a 3D block. A 3D block with numbered edges. (b) Unit tangential vector and unit normal vector



## 2.2 | Constitutive laws

Strain energy density in case of centrosymmetric materials reads

$$w(\varepsilon_{ij}, \eta_{ijk}) = \frac{1}{2} \varepsilon_{ij} C_{ijkl} \varepsilon_{kl} + \frac{1}{2} \eta_{ijk} D_{ijklmn} \eta_{lmn}, \quad (20)$$

where  $C_{ijkl}$  and  $D_{ijklmn}$  are the first and the second gradient elastic stiffness tensors, respectively. For isotropic materials, they are given by

$$C_{ijkl} = c_1 \delta_{ij} \delta_{kl} + c_2 (\delta_{ik} \delta_{jl} + \delta_{il} \delta_{jk}), \quad (21)$$

$$\begin{aligned} D_{ijklmn} = & c_3 (\delta_{ij} \delta_{kl} \delta_{mn} + \delta_{in} \delta_{jk} \delta_{lm} + \delta_{ij} \delta_{km} \delta_{ln} + \delta_{ik} \delta_{jn} \delta_{lm}) \\ & + c_4 \delta_{ij} \delta_{kn} \delta_{ml} + c_5 (\delta_{ik} \delta_{jl} \delta_{mn} + \delta_{im} \delta_{jk} \delta_{ln} + \delta_{ik} \delta_{jm} \delta_{ln} + \delta_{il} \delta_{jk} \delta_{mn}) \\ & + c_6 (\delta_{il} \delta_{jm} \delta_{kn} + \delta_{im} \delta_{jl} \delta_{kn}) + c_7 (\delta_{il} \delta_{jn} \delta_{mk} + \delta_{im} \delta_{jn} \delta_{lk} + \delta_{in} \delta_{jl} \delta_{km} + \delta_{in} \delta_{jm} \delta_{kl}). \end{aligned} \quad (22)$$

By  $c_1$  and  $c_2$  the Lamé constants are denoted. It is worth mentioning here that for a 3D case there are five additional parameters  $c_3, c_4, c_5, c_6,$  and  $c_7$  in the second gradient stiffness tensor  $D$ . By using Equations (20)–(22) we can rewrite Equation (15) as

$$\sigma_{ij} = \frac{\partial w}{\partial u_{i,j}} = c_1 \delta_{ij} \varepsilon_{kk} + 2c_2 \varepsilon_{ij}, \quad (23)$$

$$\begin{aligned} \tau_{ijk} = \frac{\partial w}{\partial u_{i,jk}} = & c_3 (\delta_{ij} \varepsilon_{km,m} + \delta_{jk} \varepsilon_{mm,i} + \delta_{ij} \varepsilon_{nk,n} + \delta_{ik} \varepsilon_{mm,j}) + c_4 \delta_{ij} \varepsilon_{ll,k} \\ & + c_5 (\delta_{ik} \varepsilon_{jn,n} + \delta_{jk} \varepsilon_{li,l} + \delta_{ik} \varepsilon_{nj,n} + \delta_{jk} \varepsilon_{im,m}) + c_6 (\varepsilon_{ij,k} + \varepsilon_{ji,k}) \\ & + c_7 (\varepsilon_{ik,j} + \varepsilon_{ki,j} + \varepsilon_{jk,i} + \varepsilon_{kj,i}). \end{aligned} \quad (24)$$

## 3 | FORMULATION OF THE PROBLEM

A 3D block, as shown in Figure 1, is considered in the current section. The motivation for this selection is twofold. First, all surface boundaries are flat, consequently, the boundary conditions are simplified. Second, the presence of sharp edges would bring the wedge forces, and their importance will be demonstrated later on. We choose the length  $l$ , width  $w$ , and height  $h$  to be equal ( $l = w = h$ ). Each of the 12 edges is characterized by a unique number, see Figure 1a. Unit tangential vectors and unit normal vectors for the right and top surfaces are presented in Figure 1b.

For the considered domain  $\Omega$  its boundary  $\partial\Omega$  is composed of flat surfaces leading to  $D_p(n_p) = 0$  on  $\partial\Omega$ . Hence Equation (18) reads

$$\begin{aligned} t_i &= n_j \sigma_{ij} - n_j (\tau_{ijk,k} + \tau_{ihj,h}) + n_j n_h n_k \tau_{ijk,h}, \\ r_i &= n_j n_k \tau_{ijk}. \end{aligned} \quad (25)$$

Thus, expressions of tractions and double tractions as well for the left surface are the following:

$$\begin{aligned} t_1^L &= -\sigma_{11} + \tau_{111,1} + \tau_{112,2} + \tau_{113,3} + \tau_{121,2} + \tau_{131,3}, \\ t_2^L &= -\sigma_{21} + \tau_{211,1} + \tau_{212,2} + \tau_{213,3} + \tau_{221,2} + \tau_{231,3}, \\ t_3^L &= -\sigma_{31} + \tau_{311,1} + \tau_{312,2} + \tau_{313,3} + \tau_{321,2} + \tau_{331,3}, \\ r_1 &= \tau_{111}, \\ r_2 &= \tau_{211}, \\ r_3 &= \tau_{311}. \end{aligned} \quad (26)$$

According to Equation (18), the so-called wedge forces are

$$f_i = \Delta v_j n_k \tau_{ijk}. \quad (27)$$

There are 12 edges in total for the 3D block. Let us take the edge number 6, which is blue in Figure 1b, as an example. The unit normal vectors and tangent vectors for the right and top surfaces are

$$\begin{aligned} n_j^R &= \delta_{1j}, & n_j^T &= \delta_{2j}, \\ v_i^R &= \delta_{i2}, & v_i^T &= \delta_{i1}. \end{aligned} \quad (28)$$

The wedge force on the edge number 6 is then calculated by

$$\begin{aligned} f_1 &= v_j^R n_k^R \tau_{1jk} + v_j^T n_k^T \tau_{1jk} = \tau_{121} + \tau_{112}, \\ f_2 &= v_j^R n_k^R \tau_{2jk} + v_j^T n_k^T \tau_{2jk} = \tau_{221} + \tau_{212}, \\ f_3 &= v_j^R n_k^R \tau_{3jk} + v_j^T n_k^T \tau_{3jk} = \tau_{321} + \tau_{312}. \end{aligned} \quad (29)$$

Expressions for tractions, double tractions, and wedge forces on the remaining surfaces and edges respectively can be calculated analogously. Expressions for the stress tensor, the hyperstress tensor, and balance equations can be given explicitly in terms of the displacement by using Equations (23), (24), and (19) as shown in Appendix.

#### 4 | ANALYTICAL AND NUMERICAL SOLUTIONS AND COMPARATIVE STUDIES OF A SECOND GRADIENT MODEL FOR A 3D BLOCK

Let us consider the deformation modes of a block corresponding to particular components of the strain gradient tensor as shown in Table 1 [6, 55]. We emphasize that for underlined indices no summation convention is applied. There are four distinct modes of deformations: Extension, torsion, non-conventional bending, and trapezoid [55, 72, 75]. These four modes correspond to specific non-zero strain gradient components, which will result in strain gradient effects of materials. For example, a trapezoid loading deforms the block to be trapezoid-shaped with non-zero strain gradient components  $\eta_{121}$  as shown in [55]. In this work, the extension, torsion, and non-conventional bending deformation modes are studied by considering specific displacement field solution corresponding to these non-zero strain gradient components as illustrated in Figure 2. The solutions of displacement fields are imposed, the corresponding boundary conditions (tractions, double tractions, and wedge forces) are found. This idea is based on the work in [9, 72, 75]. Numerical simulations are conducted

**TABLE 1** Characterization of deformation patterns associated with  $\eta$ . The summation convention is not applied over underlined indices. Unique indices are not equal ( $i \neq j, j \neq k, i \neq k$ )

Deformation patterns	Non-zero components of $\eta$
Extension	$\eta_{\underline{iii}}$
Torsion	$\eta_{\underline{ijk}}$
Non-conventional bending	$\eta_{\underline{ijj}}$
Trapezoid	$\eta_{\underline{iji}}$

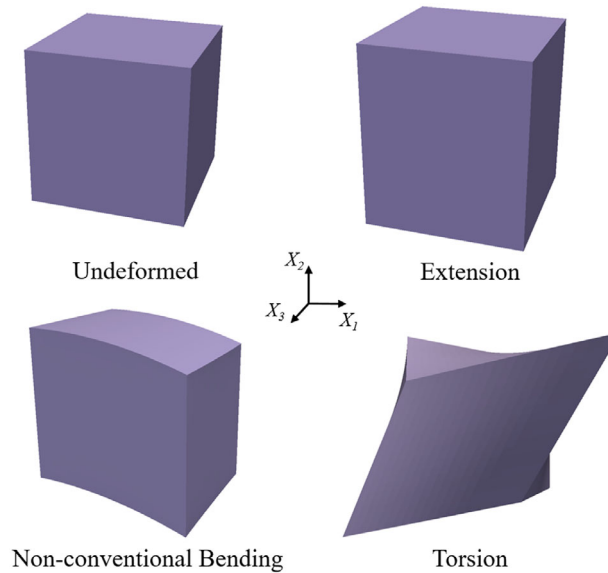


**FIGURE 2** Deformation patterns associated with non-zero  $\eta$ . Extension:  $\eta_{222}$ . Torsion:  $\eta_{123}$ . Non-conventional bending:  $\eta_{211}$

based on the derived boundary conditions, and the calculated results are compared with the displacement fields. The weak form and its numerical implementation can be found in Appendix.

The geometry sizes and constitutive parameters of the block are shown in Table 2. The values of strain gradient related parameters may be possibly given as shown in Table 2 [9]. For defining the body forces, gravitational forces are implemented by the specific force  $g=10$  N/kg. Three cases of different boundary conditions are investigated throughout this section.

### 4.1 | Extension

The following displacement fields leading to a non-zero  $\eta_{222}$  are considered:

$$u_1 = 0, \quad u_2 = \frac{\rho g(X_2 - l)(3l + X_2)}{2(c_1 + 2c_2)}, \quad u_3 = 0. \tag{30}$$

This solution of displacement fields can be achieved by the following body forces:

$$b_1 = 0, \quad b_2 = -\rho g, \quad b_3 = 0, \tag{31}$$

**TABLE 2** Numerical data used for simulations

$l$ m	$\rho$ kg/m <sup>3</sup>	$E$ Pa	$c_1$ Pa	$c_2$ Pa	$c_3$ N	$c_4$ N	$c_5$ N	$c_6$ N	$c_7$ N
0.1	$10^5$	$26 \times 10^6$	$15 \times 10^6$	$10 \times 10^6$	2600	2600	5200	2600	1300

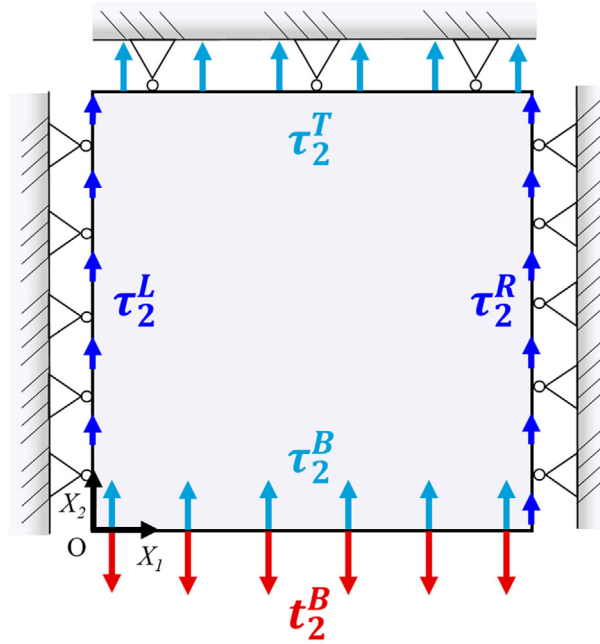


FIGURE 3 Graphical representation of the boundary conditions for the extension problem. It is visualized for a cut slice ( $z=0.05$  m)

as well as the following surface boundary conditions:

$$\begin{aligned}
 \text{Left surface: } & u_1^L = 0, \quad t_2^L = 0, \quad t_3^L = 0, \quad \tau_1^L = 0, \quad \tau_2^L = \tau_{211} = (c_3 + 2c_5) \frac{\rho g}{c_1 + 2c_2}, \quad \tau_3^L = 0, \\
 \text{Right surface: } & u_1^R = 0, \quad t_2^R = 0, \quad t_3^R = 0, \quad \tau_1^R = 0, \quad \tau_2^R = \tau_{211} = (c_3 + 2c_5) \frac{\rho g}{c_1 + 2c_2}, \quad \tau_3^R = 0, \\
 \text{Top surface: } & t_1^T = 0, \quad u_2^T = 0, \quad t_3^T = 0, \quad \tau_1^T = 0, \\
 & \tau_2^T = (4c_3 + c_4 + 4c_5 + 2c_6 + 4c_7) \frac{\rho g}{c_1 + 2c_2}, \quad \tau_3^T = 0, \\
 \text{Bottom surface: } & t_1^B = 0, \quad t_2^B = -\rho g(x_2 + l), \quad t_3^B = 0, \quad \tau_1^B = 0, \\
 & \tau_2^B = (4c_3 + c_4 + 4c_5 + 2c_6 + 4c_7) \frac{\rho g}{c_1 + 2c_2}, \quad \tau_3^B = 0, \\
 \text{Front surface: } & t_1^F = 0, \quad t_2^F = 0, \quad u_3^F = 0, \quad \tau_1^F = 0, \quad \tau_2^F = \tau_{233} = (c_3 + 2c_5) \frac{\rho g}{c_1 + 2c_2}, \quad \tau_3^F = 0, \\
 \text{Back surface: } & t_1^K = 0, \quad t_2^K = 0, \quad u_3^K = 0, \quad \tau_1^K = 0, \quad \tau_2^K = \tau_{233} = (c_3 + 2c_5) \frac{\rho g}{c_1 + 2c_2}, \quad \tau_3^K = 0.
 \end{aligned} \tag{32}$$

Due to the kinematic restrictions, the wedge forces are not imposed in this case. The imposed kinematical constraints and boundary conditions are also shown in Figure 3 for a cut slice. Plots for numerically obtained total displacement are presented in Figure 4. In Figure 5, perfect overlap is observed between the analytical and numerical results. A difference is shown for numerical solutions if double tractions are not taken into account.

## 4.2 | Torsion

Lets now consider a torsion problem with the following displacement fields:

$$u_1 = TX_2X_3, \quad u_2 = TX_1X_3, \quad u_3 = TX_1X_2, \tag{33}$$



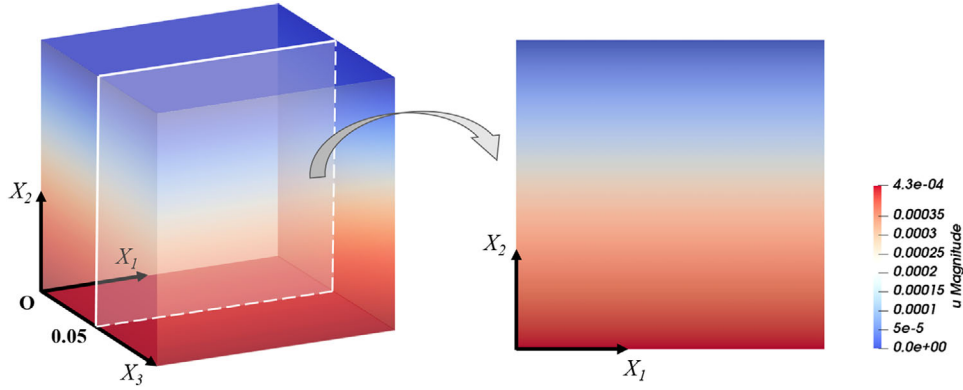


FIGURE 4 Total displacement of the extensional case

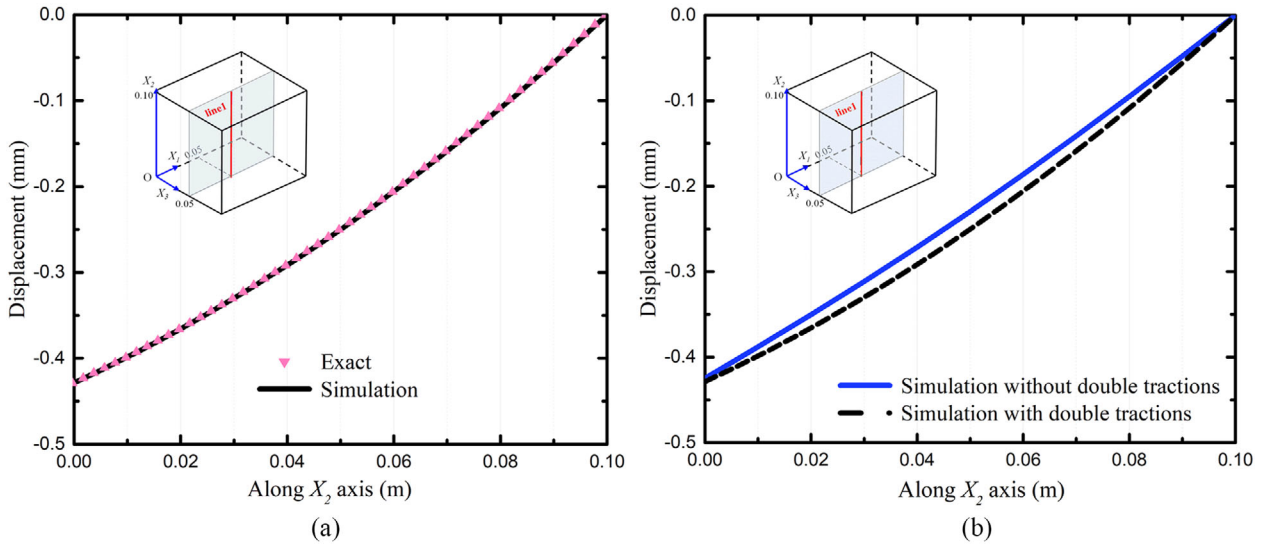


FIGURE 5 Comparisons for analytical solution and numerical ones. (a) Comparisons between the exact solution and the numerical one through a cut along  $X_2$ . (b) Comparisons between simulations through a cut along  $X_2$

where  $T$  is a small constant with the physical dimension of the inverse of a length ( $T$  is set to be equal to  $0.1 \text{ m}^{-1}$ ). The analytical solution is achieved by the following body forces:

$$b_1 = 0, \quad b_2 = 0, \quad b_3 = 0, \tag{34}$$

as well as the following boundary conditions:

$$\begin{aligned} \text{Left surface: } & t_1^L = 0, u_2^L = 0, u_3^L = 0, \tau_1^L = 0, \tau_2^L = 0, \tau_3^L = 0, \\ \text{Right surface: } & t_1^R = 0, t_2^R = 2Tc_2X_3, t_3^R = 2Tc_2X_2, \tau_1^R = 0, \tau_2^R = 0, \tau_3^R = 0, \\ \text{Top surface: } & t_1^T = -2Tc_2X_3, t_2^T = 0, t_3^T = 2Tc_2X_1, \tau_1^T = 0, \tau_2^T = 0, \tau_3^T = 0, \\ \text{Bottom surface: } & u_1^B = 0, t_2^B = 0, u_3^B = 0, \tau_1^B = 0, \tau_2^B = 0, \tau_3^B = 0, \\ \text{Front surface: } & t_1^F = 2Tc_2X_2, t_2^F = 2Tc_2X_1, t_3^F = 0, \tau_1^F = 0, \tau_2^F = 0, \tau_3^F = 0, \\ \text{Back surface: } & u_1^K = 0, u_2^K = 0, t_3^K = 0, \tau_1^K = 0, \tau_2^K = 0, \tau_3^K = 0. \end{aligned} \tag{35}$$

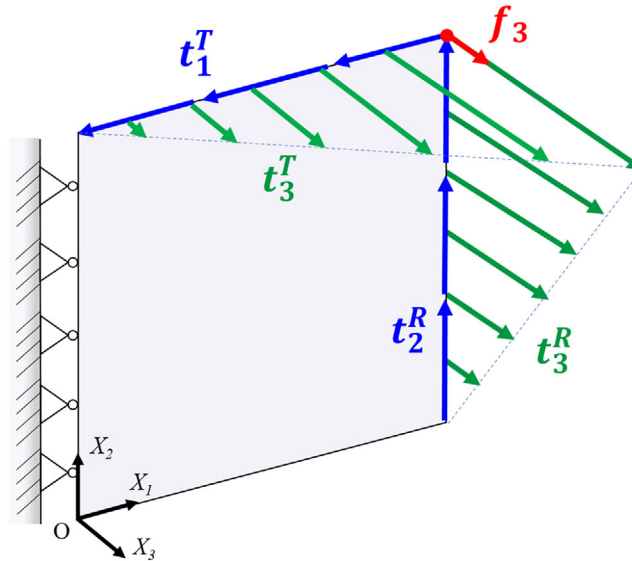


FIGURE 6 Graphical representation of the boundary conditions for the torsion problem. It is visualized for a cut slice ( $z = 0.05$  m)

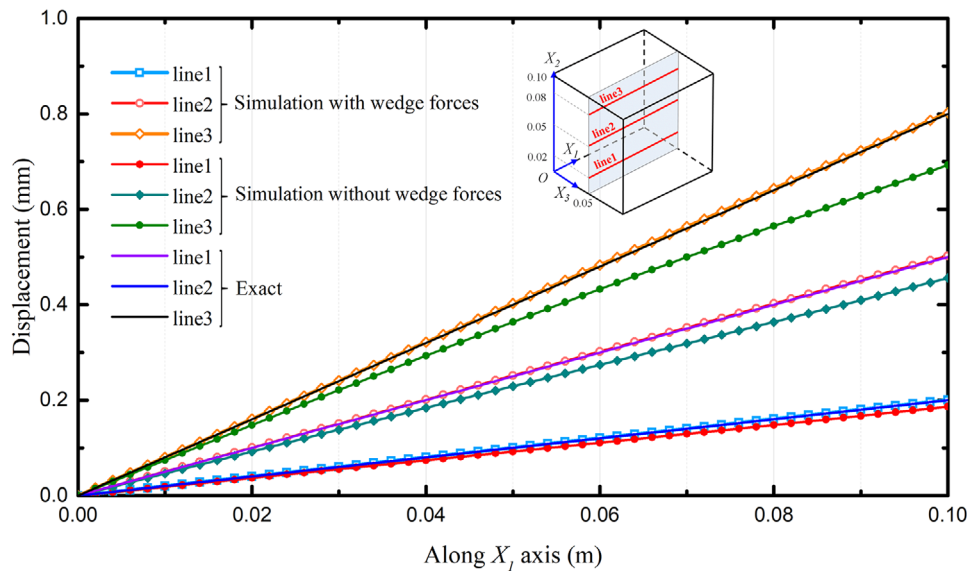


FIGURE 7 Comparisons between the exact solution and the numerical ones through three different cut

We emphasize that the double tractions on all of the surfaces are equal to zero. According to the kinematical restrictions, the imposed non-zero wedge forces are calculated by Equation (27)

$$\text{Edge 2: } f_1 = \tau_{132} + \tau_{123} = T(4c_6 + 8c_7),$$

$$\text{Edge 3: } f_2 = \tau_{213} + \tau_{231} = T(4c_6 + 8c_7), \quad (36)$$

$$\text{Edge 6: } f_3 = \tau_{321} + \tau_{312} = T(4c_6 + 8c_7).$$

Figure 6 presents the imposed kinematical constraints and boundary conditions for a cut slice. Comparing the exact solution with the numerical outcomes on three different cuts (line1, line2, line3), see Figure 7, we observe that the plot for simulation incorporating wedge forces demonstrate an almost perfect overlapping with the plot of the analytical solution. Figure 8 indicates differences for total displacement plots for different boundary conditions. It is well known that a sin-

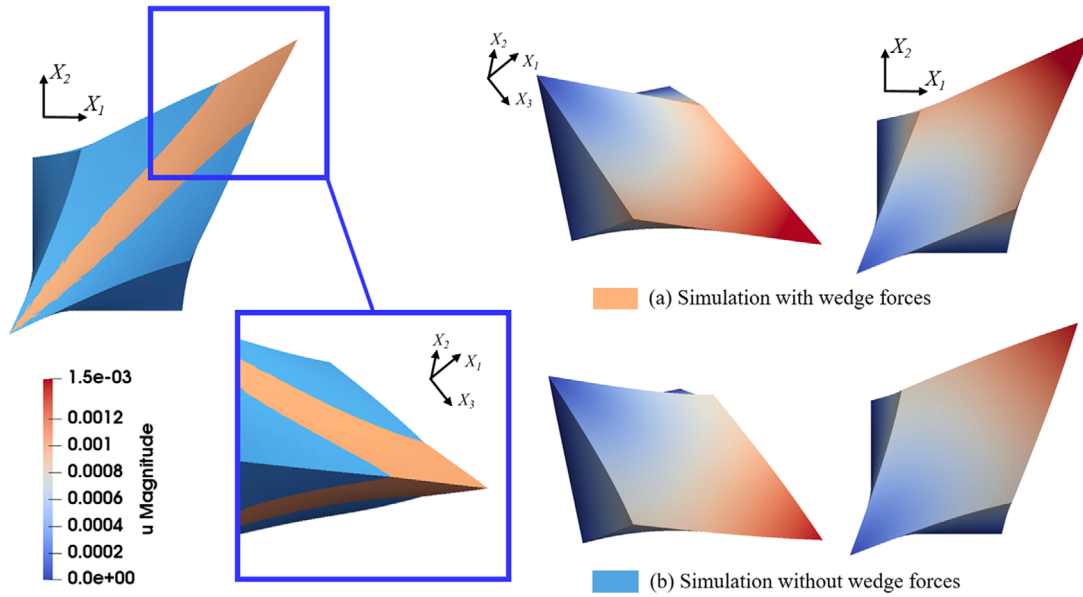


FIGURE 8 Comparisons between numerical solutions for the torsion tests (Scaling factor = 40). On the left hand side, the blocks are presented in the current configuration by two different colors for these two different numerical solutions

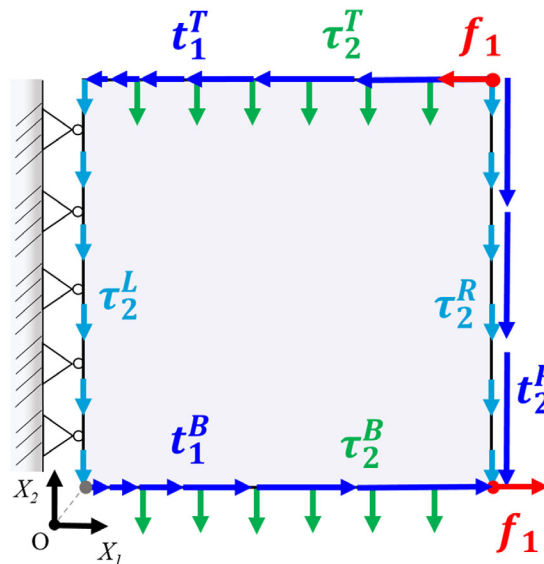


FIGURE 9 Graphical representation of the boundary conditions for the non-conventional bending problem. It is visualized for a cut slice ( $z=0.05$  m)

gularity results under line loads for classical Cauchy continuum. However, the line loads (or wedge forces) in the strain gradient continuum are necessary and yield a continuous solution for the displacement fields.

### 4.3 | Non-conventional bending

The so-called non-conventional bending problem is considered. The displacement field equations are conceived as

$$u_1 = 0, \quad u_2 = -B \frac{X_1^2}{2}, \quad u_3 = 0, \tag{37}$$

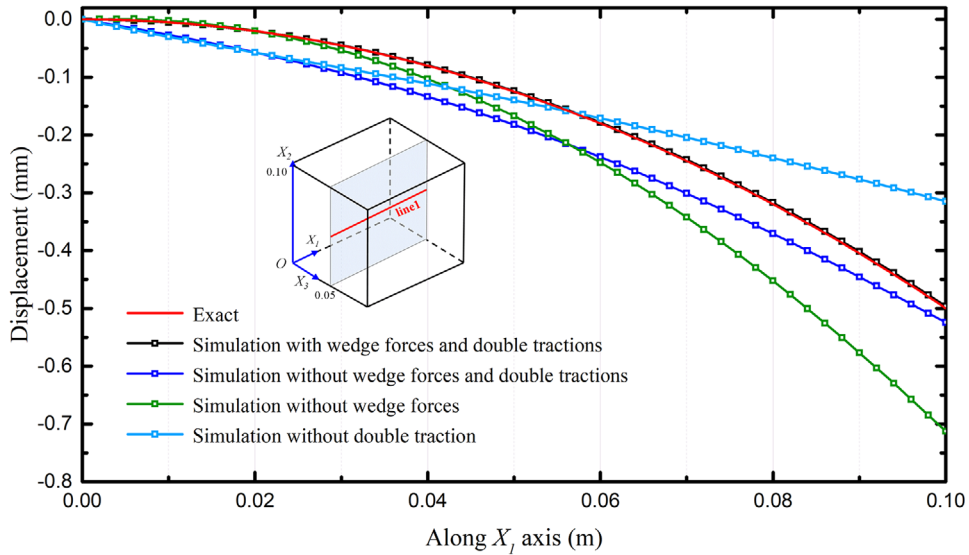


FIGURE 10 Comparisons between the exact solution and the numerical ones through a cut indicated as line 1

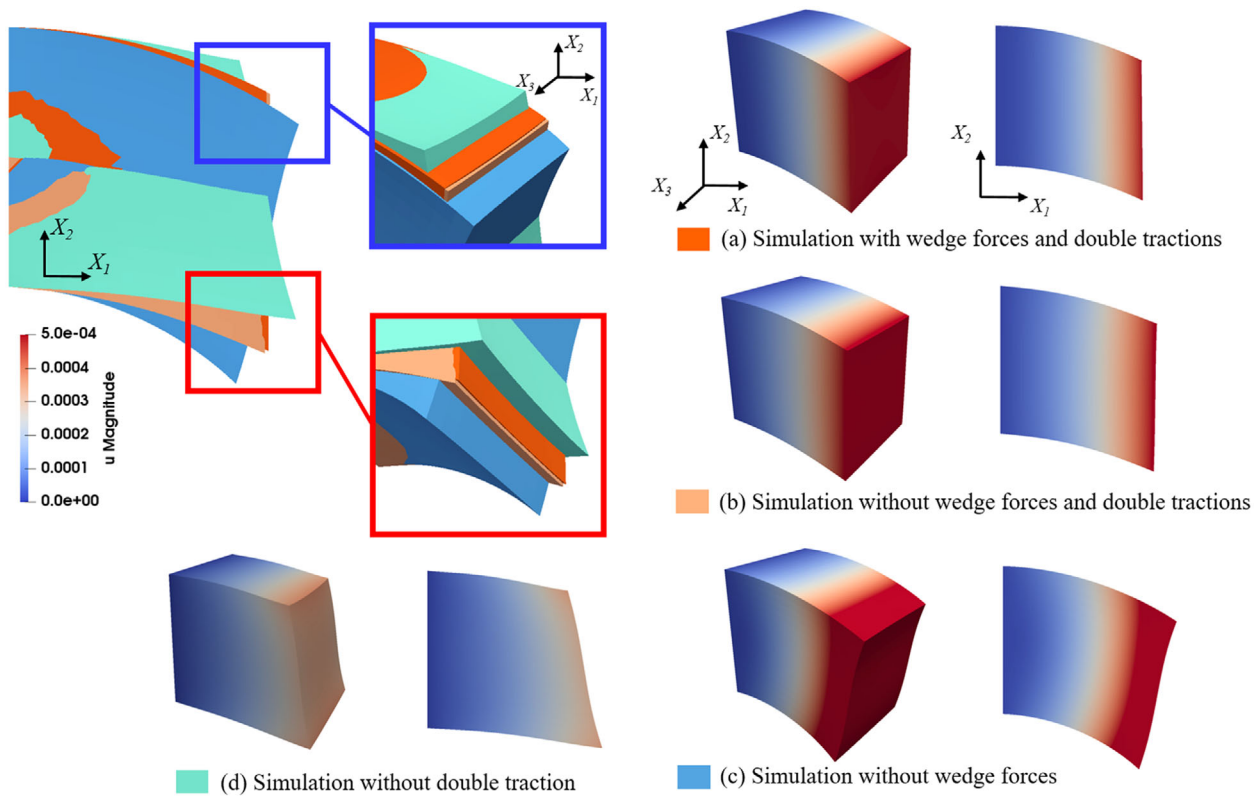


FIGURE 11 Total displacement for the non-conventional bending problem (scaling factor 50). Four different colors are used to demonstrate differences of the numerical solutions on the left hand side

where  $B$  is a small constant with the physical dimension of the inverse of a length ( $B$  is set to be equal to  $0.1 \text{ m}^{-1}$ ). The solution of the displacement field is acquired by the following body forces:

$$b_1 = 0, \quad b_2 = Bc_2, \quad b_3 = 0, \tag{38}$$

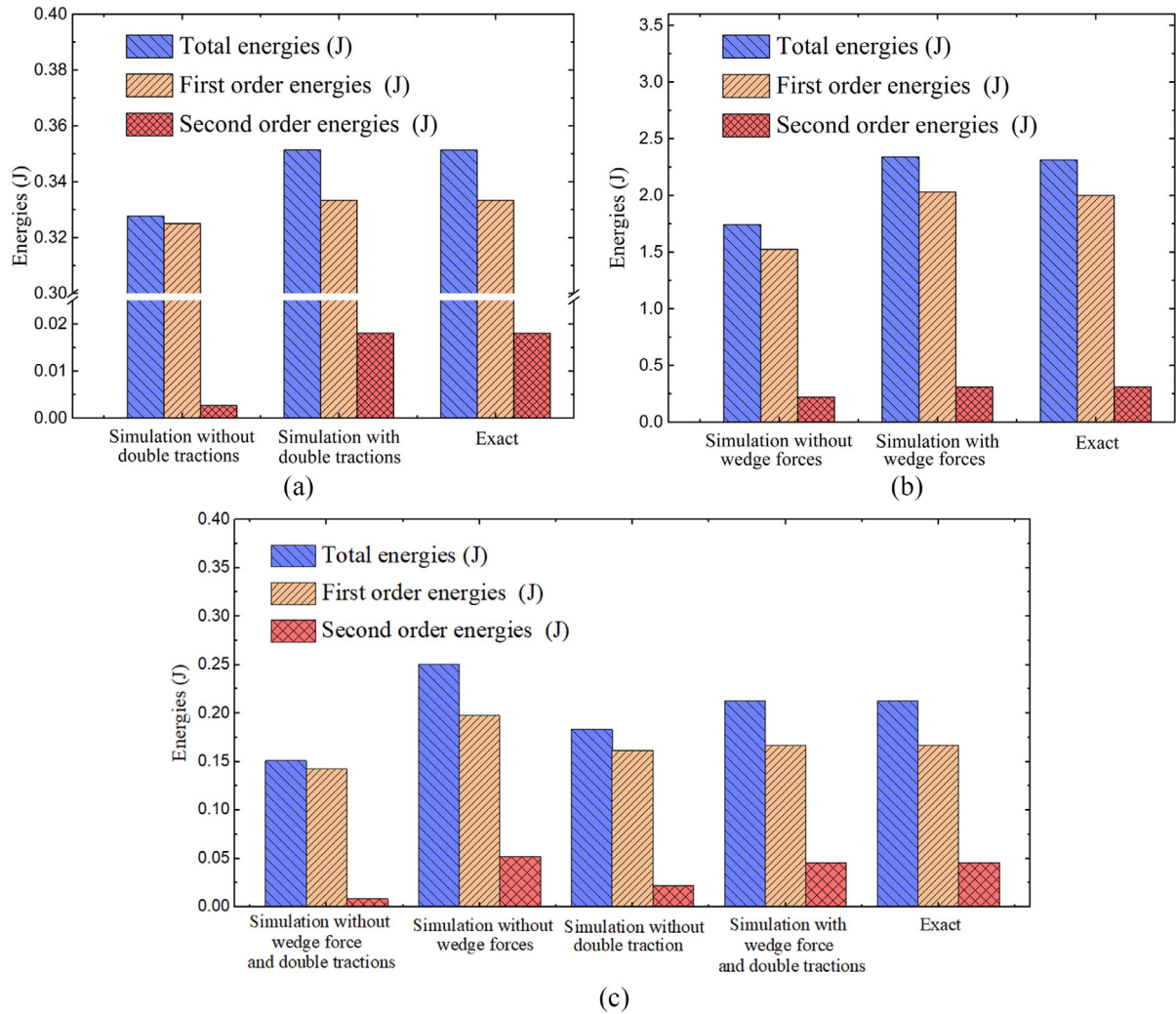


FIGURE 12 Comparisons for strain energies among analytical solutions and numerical ones. (a) Strain energies for the extensional case. (b) Strain energies for the torsion case. (c) Strain energies for the non-conventional bending case

as well as the following boundary conditions:

$$\begin{aligned}
 \text{Left surface: } & u_1^L = 0, u_2^L = 0, u_3^L = 0, \tau_1^L = 0, \tau_2^L = \tau_{211} = (-B)(c_5 + c_6 + c_7), \tau_3^L = 0, \\
 \text{Right surface: } & t_1^R = 0, t_2^R = -Bc_2X_1, t_3^R = 0, \tau_1^R = 0, \tau_2^R = (-B)(c_5 + c_6 + c_7), \tau_3^R = 0, \\
 \text{Top surface: } & t_1^T = -Bc_2X_1, t_2^T = 0, t_3^T = 0, \tau_1^T = 0, \tau_2^T = (-B)(c_3 + 2c_5), \tau_3^T = 0, \\
 \text{Bottom surface: } & t_1^B = Bc_2X_1, t_2^B = 0, t_3^B = 0, \tau_1^B = 0, \tau_2^B = (-B)(c_3 + 2c_5), \tau_3^B = 0, \\
 \text{Front surface: } & t_1^F = 0, t_2^F = 0, t_3^F = 0, \tau_1^F = 0, \tau_2^F = -Bc_5, \tau_3^F = 0, \\
 \text{Back surface: } & t_1^K = 0, t_2^K = 0, t_3^K = 0, \tau_1^K = 0, \tau_2^K = -Bc_5, \tau_3^K = 0.
 \end{aligned} \tag{39}$$

The following wedge forces calculated by Equation (27) are imposed

$$\begin{aligned}
 \text{Edge 2: } & f_3 = \tau_{332} + \tau_{323} = (-B)(c_3 + c_5), \\
 \text{Edge 4: } & f_3 = \tau_{121} + \tau_{112} = B(c_3 + c_5), \\
 \text{Edge 6: } & f_1 = \tau_{121} + \tau_{112} = (-B)(c_3 + c_5 + c_6 + 3c_7),
 \end{aligned}$$

$$\text{Edge 7: } f_1 = -\tau_{121} - \tau_{112} = B(c_3 + c_5 + c_6 + 3c_7),$$

$$\text{Edge 10: } f_3 = -\tau_{332} - \tau_{323} = (-B)(c_3 + c_5),$$

$$\text{Edge 12: } f_3 = \tau_{332} + \tau_{323} = B(c_3 + c_5). \quad (40)$$

The imposed kinematical constraints and boundary conditions are presented in Figure 9 for a cut slice.

A comparison between the analytical solutions and the numerical ones along a line cut (line 1) are shown in Figure 10. Obviously, when the double tractions and wedge forces are both imposed, the numerical results are in good agreement with the analytical solutions as also observed in Figure 11.

The strain energies are calculated and presented here for the analytical and numerical solutions as shown in Figure 12. First order  $\frac{1}{2}\varepsilon_{ij}C_{ijkl}\varepsilon_{kl}$  and second order  $\frac{1}{2}\eta_{ijk}D_{ijklmn}\eta_{lmn}$  energies contribute differently in different cases. With the correctly imposed boundaries conditions the strain energies of the numerical solutions show an adequate agreement with the analytical solutions.

## 5 | CONCLUSIONS

In this paper, numerical simulations based on IGA are performed in order to be compared with an analytical solution obtained using the inverse method. Three exemplary cases of different boundary conditions were considered in 3D: Extension, torsion, and non-conventional bending. Numerical simulations were performed with and without taking the so-called wedge forces and double tractions into account. It was shown that the numerical results are in good agreement with the analytical solutions if the wedge forces and double tractions are considered. Besides that, we presented comparisons between the numerical simulations. Such a comparison helps to reveal and comprehend the roles of the wedge forces and double tractions in the solutions. The numerical implementation was conducted by means of an open source tool called tIGAr which is based on FEniCS library.

## ACKNOWLEDGMENTS

Open access funding enabled and organized by Projekt DEAL.

## ORCID

Hua Yang  <https://orcid.org/0000-0003-2080-3452>

B. Emek Abali  <https://orcid.org/0000-0002-8735-6071>

## REFERENCES

- [1] Abali, B.E.: Revealing the physical insight of a length-scale parameter in metamaterials by exploiting the variational formulation. *Contin. Mech. Thermodyn.* 31(4), 885–894 (2019)
- [2] Abali, B.E.: Supply code for computations. <http://bilenemek.abali.org/> (2020)
- [3] Abali, B.E., Barchiesi, E.: Additive manufacturing introduced substructure and computational determination of metamaterials parameters by means of the asymptotic homogenization. *Contin. Mech. Thermodyn.* 33, 1–17 (2020)
- [4] Abali, B.E., Müller, W.H., dell’Isola, F.: Theory and computation of higher gradient elasticity theories based on action principles. *Arch. Appl. Mech.* 87(9), 1495–1510 (2017)
- [5] Abali, B.E., Müller, W.H., Eremeyev, V.A.: Strain gradient elasticity with geometric nonlinearities and its computational evaluation. *Mech. Adv. Mater. Mod. Process.* 1(1), 1–11 (2015)
- [6] Abali, B.E., Yang, H., Papadopoulos, P.: A computational approach for determination of parameters in generalized mechanics. In *Higher Gradient Materials and Related Generalized Continua*, pp. 1–18. Springer (2019)
- [7] Abdoul-Anziz, H., Seppecher, P.: Strain gradient and generalized continua obtained by homogenizing frame lattices. *Math Mechanics Complex Systems* 6(3), 213–250 (2018)
- [8] Alibert, J.-J., Seppecher, P., dell’Isola, F.: Truss modular beams with deformation energy depending on higher displacement gradients. *Math. Mech. Solids* 8(1), 51–73 (2003)
- [9] Andraus, U., dell’Isola, F., Giorgio, I., Placidi, L., Lekszycki, T., Rizzi, N.L.: Numerical simulations of classical problems in two-dimensional (non) linear second gradient elasticity. *Int. J. Eng. Sci.* 108, 34–50 (2016)
- [10] Auffray, N., dell’Isola, F., Eremeyev, V.A., Madeo, A., Rosi, G.: Analytical continuum mechanics à la Hamilton–Piola least action principle for second gradient continua and capillary fluids. *Math. Mech. Solids* 20(4), 375–417 (2015)
- [11] Auffray, N., Dirrenberger, J., Rosi, G.: A complete description of bi-dimensional anisotropic strain-gradient elasticity. *Int. J. Solids Struct.* 69, 195–206 (2015)

- [12] Barchiesi, E., dell'Isola, F., Hild, F., Seppecher, P.: Two-dimensional continua capable of large elastic extension in two independent directions: Asymptotic homogenization, numerical simulations and experimental evidence. *Mech. Res. Commun.* 103, 103466 (2020)
- [13] Barchiesi, E., Eugster, S.R., dell'Isola, F., Hild, F.: Large in-plane elastic deformations of bi-pantographic fabrics: Asymptotic homogenization and experimental validation. *Math. Mech. Solids* 25(3), 739–767 (2020)
- [14] Barchiesi, E., Eugster, S.R., Placidi, L., dell'Isola, F.: Pantographic beam: a complete second gradient 1d-continuum in plane. *Z. Angew. Math. Phys.* 70(5), 135 (2019)
- [15] Barchiesi, E., Ganzosch, G., Liebold, C., Placidi, L., Grygoruk, R., Müller, W.H.: Out-of-plane buckling of pantographic fabrics in displacement-controlled shear tests: experimental results and model validation. *Contin. Mech. Thermodyn.* 31(1), 33–45 (2019)
- [16] Barchiesi, E., Spagnuolo, M., Placidi, L.: Mechanical metamaterials: a state of the art. *Math. Mech. Solids* 24(1), 212–234 (2019)
- [17] Barchiesi, E., Yang, H., Tran, C., Placidi, L., Müller, W.: Computation of brittle fracture propagation in strain gradient materials by the FEniCS library. *Math. Mech. Solids* 1081286520954513 (2020)
- [18] Bertram, A.: Balance laws for gradient materials. In *Mechanics of Strain Gradient Materials*, pp. 19–35. Springer (2020)
- [19] Cazzani, A., Malagù, M., Turco, E.: Isogeometric analysis: A powerful numerical tool for the elastic analysis of historical masonry arches. *Contin. Mech. Thermodyn.* 28(1-2), 139–156 (2016)
- [20] Cazzani, A., Malagù, M., Turco, E.: Isogeometric analysis of plane-curved beams. *Math. Mech. Solids* 21(5), 562–577 (2016)
- [21] Cazzani, A., Stochino, F., Turco, E.: An analytical assessment of finite element and isogeometric analyses of the whole spectrum of Timoshenko beams. *ZAMM - J. Appl. Math. Mech./Z. Angew. Math. Mech.* 96(10), 1220–1244 (2016)
- [22] Charalambopoulos, A., Tsinopoulos, S.V., Polyzos, D.: Plane strain gradient elastic rectangle in bending. *Arch. Appl. Mech.* 1–20 (2020)
- [23] Chen, Q., Chen, W., Wang, G.: Fully-coupled electro-magneto-elastic behavior of unidirectional multiphased composites via finite-volume homogenization. *Mech. Mater.* 103553 (2020)
- [24] De Angelo, M., Barchiesi, E., Giorgio, I., Abali, B.E.: Numerical identification of constitutive parameters in reduced-order bi-dimensional models for pantographic structures: application to out-of-plane buckling. *Arch. Appl. Mech.* 89(7), 1333–1358 (2019)
- [25] De Angelo, M., Spagnuolo, M., D'annibale, F., Pfaff, A., Hoschke, K., Misra, A., Dupuy, C., Peyre, P., Dirrenberger, J., Pawlikowski, M.: The macroscopic behavior of pantographic sheets depends mainly on their microstructure: experimental evidence and qualitative analysis of damage in metallic specimens. *Contin. Mech. Thermodyn.* 31(4), 1181–1203 (2019)
- [26] Del, Vescovo, D., Giorgio, I.: Dynamic problems for metamaterials: review of existing models and ideas for further research. *Int. J. Eng. Sci.* 80, 153–172 (2014)
- [27] dell'Isola, F., Andreaus, U., Luca, P.: At the origins and in the vanguard of peri-dynamics, non-local and higher gradient continuum mechanics. an underestimated and still topical contribution of Gabrio Piola. *Math. Mech. Solids* 20(8), 887–928 (2015)
- [28] dell'Isola, F., Bucci, S., Battista, A.: Against the fragmentation of knowledge: the power of multidisciplinary research for the design of metamaterials. *Adv. Methods Continuum Mechanics for Materials Struct.* 523–545 (2016)
- [29] dell'Isola, F., Della Corte, A., Giorgio, I.: Higher-gradient continua: The legacy of Piola, Mindlin, Sedov and Toupin and some future research perspectives. *Math. Mech. Solids* 22(4), 852–872 (2017)
- [30] dell'Isola, F., Placidi, L.: Variational principles are a powerful tool also for formulating field theories. *Variational models and methods in solid and fluid mechanics* 1–15 (2012)
- [31] dell'Isola, F., Sciarra, G., Vidoli, S.: Generalized Hooke's law for isotropic second gradient materials. In *Proceedings of the Royal Society of London A: Mathematical, Physical and Engineering Sciences* rspa–2008. The Royal Society (2009)
- [32] dell'Isola, F., Seppecher, P., Alibert, J.J., Lekszycki, T., et al.: Pantographic metamaterials: An example of mathematically driven design and of its technological challenges. *Contin. Mech. Thermodyn.* 31(4), 851–884 (2019)
- [33] dell'Isola, F., Seppecher, P., Madeo, A.: How contact interactions may depend on the shape of cauchy cuts in Nth gradient continua: Approach “à la D'Alembert”. *Z. Angew. Math. Phys.* 63(6), 1119–1141 (2012)
- [34] dell'Isola, F., Seppecher, P., Spagnuolo, M., Barchiesi, E., et al.: Advances in pantographic structures: design, manufacturing, models, experiments and image analyses. *Contin. Mech. Thermodyn.* 31(4), 1231–1282 (2019)
- [35] dell'Isola, F., Steigmann, D., Della Corte, A.: Synthesis of fibrous complex structures: Designing microstructure to deliver targeted macroscale response. *Appl. Mech. Rev.* 67(6), 060804 (2015)
- [36] Eremeyev, V.A., dell'Isola, F.: A note on reduced strain gradient elasticity. *Generalized Models and Non-classical Approaches in Complex Materials* 1, 301–310 (2018)
- [37] Eremeyev, V.A., Lebedev, L.P., Altenbach, H.: *Foundations of Micropolar Mechanics*. Springer Science & Business Media (2012)
- [38] Eugster, S., dell'Isola, F., Steigmann, D.: Continuum theory for mechanical metamaterials with a cubic lattice substructure. *Mathematics and Mechanics of Complex Systems* 7(1), 75–98 (2019)
- [39] Fischer, P., Klassen, M., Mergheim, J., Steinmann, P., Müller, R.: Isogeometric analysis of 2D gradient elasticity. *Computational Mechanics* 47(3), 325–334 (2011)
- [40] Giorgio, I.: Lattice shells composed of two families of curved kirchhoff rods: An archetypal example, topology optimization of a cycloidal metamaterial. *Contin. Mech. Thermodyn.* 1–20 (2020)
- [41] Giorgio, I., Rizzi, N., Turco, E.: Continuum modelling of pantographic sheets for out-of-plane bifurcation and vibrational analysis. *Proc. R. Soc. Lond. A, Math. Phys. Eng. Sci.* 473(2207), 20170636 (2017)
- [42] Glüge, R.: A for C strain I incompatible gradient mode elasticity element formulation. *Higher Gradient Materials and Related Generalized Continua* 120, 95 (2019)
- [43] Glüge, R., Altenbach, H., Mahmood, N., Beiner, M.: On the difference between the tensile stiffness of bulk and slice samples of microstructured materials. *Appl. Compos. Mater.* 1–20 (2020)

- [44] Gnu Public: Gnu general public license. <http://www.gnu.org/copyleft/gpl.html> (2007)
- [45] Golaszewski, M., Grygoruk, R., Giorgio, I., Laudato, M., Di Cosmo, F.: Metamaterials with relative displacements in their microstructure: Technological challenges in 3d printing, experiments and numerical predictions. *Contin. Mech. Thermodyn.* 31(4), 1015–1034 (2019)
- [46] Hughes, T.J., Cottrell, J.A., Bazilevs, Y.: Isogeometric analysis: CAD, finite elements, NURBS, exact geometry and mesh refinement. *Comput. Methods Appl. Mech. Eng.* 194(39–41), 4135–4195 (2005)
- [47] Hutchinson, J., Fleck, N.: Strain gradient plasticity. *Advances in Applied Mechanics* 33, 295–361 (1997)
- [48] Javii, A., Steinmann, P., dell’Isola, F.: Geometrically nonlinear higher-gradient elasticity with energetic boundaries. *J. Mech. Phys. Solids* (2013)
- [49] Kamensky, D.: Open-source immersogeometric analysis of fluid–structure interaction using FEniCS and tIGAr. *Comput. Math. Appl.* (2020)
- [50] Kamensky, D., Bazilevs, Y.: tIGAr: Automating isogeometric analysis with FEniCS. *Comput. Methods Appl. Mech. Eng.* 344, 477–498 (2019)
- [51] Khakalo, S., Niiranen, J.: Anisotropic strain gradient thermoelasticity for cellular structures: Plate models, homogenization and isogeometric analysis. *J. Mech. Phys. Solids* 134, 103728 (2020)
- [52] Lam, D.C., Yang, F., Chong, A., Wang, J., Tong, P.: Experiments and theory in strain gradient elasticity. *J. Mech. Phys. Solids* 51(8), 1477–1508 (2003)
- [53] Liu, H., Li, B., Yang, Z., Hong, J.: Topology optimization of stiffened plate/shell structures based on adaptive morphogenesis algorithm. *J. Manuf. Syst.* 43, 375–384 (2017)
- [54] Liu, H., Li, B., Zhang, L., Li, X.: Optimizing heat-absorption efficiency of phase change materials by mimicking leaf vein morphology. *Appl. Energy* 269, 114982 (2020)
- [55] Luscher, D.J., McDowell, D.L., Bronkhorst, C.A.: A second gradient theoretical framework for hierarchical multiscale modeling of materials. *Int. J. Plast.* 26(8), 1248–1275 (2010)
- [56] Makvandi, R., Reiher, J.C., Bertram, A., Juhre, D.: Isogeometric analysis of first and second strain gradient elasticity. *Comput. Mech.* 61(3), 351–363 (2018)
- [57] Mandadapu, K.K., Abali, B.E., Papadopoulos, P.: On the polar nature and invariance properties of a thermomechanical theory for continuum-on-continuum homogenization. *arXiv preprint arXiv:1808.02540* (2018)
- [58] Mindlin, R.D.: Micro-structure in linear elasticity. *Arch. Ration. Mech. Anal.* 16(1), 51–78 (1964)
- [59] Mindlin, R.D.: Second gradient of strain and surface-tension in linear elasticity. *Int. J. Solids Struct.* 1(4), 417–438 (1965)
- [60] Misra, A., Lekszycki, T., Giorgio, I., Ganzosch, G., Müller, W.H., dell’Isola, F.: Pantographic metamaterials show atypical poynting effect reversal. *Mech. Res. Commun.* 89, 6–10 (2018)
- [61] Müller, W.H.: The experimental evidence for higher gradient theories. In *Mechanics of Strain Gradient Materials*, pp. 1–18. Springer (2020)
- [62] Müller, W.H., Rickert, W., Vilchevskaia, E.N.: Thence the moment of momentum. *ZAMM - J. Appl. Math. Mech./Zeitschrift für Angewandte Mathematik und Mechanik* 100(5), e202000117 (2020)
- [63] Nazarenko, L., Glüge, R., Altenbach, H.: Positive definiteness in coupled strain gradient elasticity. *Contin. Mech. Thermodyn.* 1–13 (2020)
- [64] Neff, P., Ghiba, I.-D., Madeo, A., Placidi, L., Rosi, G.: A unifying perspective: The relaxed linear micromorphic continuum. *Contin. Mech. Thermodyn.* 26(5), 639–681 (2014)
- [65] NejadSadeghi, N., De Angelo, M., Drobnicki, R., Lekszycki, T., dell’Isola, F., Misra, A.: Parametric experimentation on pantographic unit cells reveals local extremum configuration. *Exp. Mech.* 59(6), 927–939 (2019)
- [66] Papanicolopoulos, S.-A., Zervos, A., Vardoulakis, I.: A three-dimensional C1 finite element for gradient elasticity. *Int. J. Numer. Methods Eng.* 77(10), 1396–1415 (2009)
- [67] Phunpeng, V., Baiz, P.: Mixed finite element formulations for strain-gradient elasticity problems using the FEniCS environment. *Finite Elem. Anal. Des.* 96, 23–40 (2015)
- [68] Placidi, L.: A variational approach for a nonlinear one-dimensional damage-elasto-plastic second-gradient continuum model. *Contin. Mech. Thermodyn.* 28, 119–137 (2016)
- [69] Placidi, L., Andreaus, U., Della Corte, A., Lekszycki, T.: Gedanken experiments for the determination of two-dimensional linear second gradient elasticity coefficients. *Z. Angew. Math. Phys.* 66(6), 3699–3725 (2015)
- [70] Placidi, L., Andreaus, U., Giorgio, I.: Identification of two-dimensional pantographic structure via a linear D4 orthotropic second gradient elastic model. *J. Eng. Math.* 103(1), 1–21 (2017)
- [71] Placidi, L., Barchiesi, E.: Energy approach to brittle fracture in strain-gradient modelling. *Proc. R. Soc. Lond. A, Math. Phys. Eng. Sci.* 474(2210), 20170878 (2018)
- [72] Placidi, L., Barchiesi, E., Battista, A.: An inverse method to get further analytical solutions for a class of metamaterials aimed to validate numerical integrations. In: dell’Isola, F., Sofonea, M., Steigmann, D. (Eds) *Mathematical Modelling in Solid Mechanics*, volume 69 of *Advanced Structured Materials*, pp. 193–210. Springer Singapore (2017)
- [73] Placidi, L., Barchiesi, E., Misra, A.: A strain gradient variational approach to damage: A comparison with damage gradient models and numerical results. *Mathematics and Mechanics of Complex Systems* 6(2), 77–100 (2018)
- [74] Placidi, L., El Dhaba, A.R.: Semi-inverse method à la Saint-Venant for two-dimensional linear isotropic homogeneous second-gradient elasticity. *Math. Mech. Solids* 22(5), 919–937 (2017)
- [75] Placidi, L., Rosi, G., Barchiesi, E.: Analytical solutions of 2-dimensional second gradient linear elasticity for continua with cubic  $D_4$  microstructure. In: Abali, B., Altenbach, H., dell’Isola, F., Eremeyev, V., Öchsner, A. (Eds) *New Achievements in Continuum Mechanics and Thermodynamics*, volume 108 of *Advanced Structured Materials*, pp. 383–401. Springer, Cham (2019)



- [76] Placidi, L., Rosi, G., Giorgio, I., Madeo, A.: Reflection and transmission of plane waves at surfaces carrying material properties and embedded in second-gradient materials. *Math. Mech. Solids* 19(5), 555–578 (2014)
- [77] Reiher, J.C., Giorgio, I., Bertram, A.: Finite-element analysis of polyhedra under point and line forces in second-strain gradient elasticity. *Journal of Engineering Mechanics* 143(2), 04016112 (2017)
- [78] Rinaldi, A., Placidi, L.: A microscale second gradient approximation of the damage parameter of quasi-brittle heterogeneous lattices. *Z. Angew. Math. Mech.* 94(10), 862–877 (2014)
- [79] Roache, P.J.: Code verification by the method of manufactured solutions. *J. Fluids Eng.* 124(1), 4–10 (2002)
- [80] Rosi, G., Auffray, N.: Anisotropic and dispersive wave propagation within strain-gradient framework. *Wave Motion* 63, 120–134 (2016)
- [81] Rudraraju, S., Van der Ven, A., Garikipati, K.: Three-dimensional isogeometric solutions to general boundary value problems of Toupin's gradient elasticity theory at finite strains. *Comput. Methods Appl. Mech. Eng.* 278, 705–728 (2014)
- [82] Schulte, J., Dittmann, M., Eugster, S., Hesch, S., Reinicke, T., dell'Isola, F., Hesch, C.: Isogeometric analysis of fiber reinforced composites using Kirchhoff–Love shell elements. *Comput. Methods Appl. Mech. Eng.* 362, 112845 (2020)
- [83] Seppacher, P., Alibert, J.-J., dell'Isola, F.: Linear elastic trusses leading to continua with exotic mechanical interactions. *Journal of Physics: Conference Series* 319(1), 012018 (2011)
- [84] Shekarchizadeh, N., Abali, B.E., Barchiesi, E., Bersani, A.M.: Inverse analysis of metamaterials and parameter determination by means of an automatized optimization problem. *ZAMM - J. Appl. Math. Mech. / Zeitschrift für Angewandte Mathematik und Mechanik* e202000277 (2021)
- [85] Shu, J.Y., King, W.E., Fleck, N.A.: Finite elements for materials with strain gradient effects. *Int. J. Numer. Methods Eng.* 44(3), 373–391 (1999)
- [86] Solyaev, Y., Lurie, S., Barchiesi, E., Placidi, L.: On the dependence of standard and gradient elastic material constants on a field of defects. *Math. Mech. Solids* 25(1), 35–45 (2020)
- [87] Tran, C.A., Gołaszewski, M., Barchiesi, E.: Symmetric-in-plane compression of polyamide pantographic fabrics—modelling, experiments and numerical exploration. *Symmetry* 12(5), 693 (2020)
- [88] Turco, E., Barchiesi, E.: Equilibrium paths of Hencky pantographic beams in a three-point bending problem. *Mathematics and Mechanics of Complex Systems* 7(4), 287–310 (2019)
- [89] Turco, E., Barchiesi, E., Giorgio, I., dell'Isola, F.: A Lagrangian Hencky-type non-linear model suitable for metamaterials design of shearable and extensible slender deformable bodies alternative to Timoshenko theory. *Int. J. Non-Linear Mech.* 123, 103481 (2020)
- [90] Yang, H., Abali, B.E., Timofeev, D., Müller, W.H.: Determination of metamaterial parameters by means of a homogenization approach based on asymptotic analysis. *Contin. Mech. Thermodyn.* 1–20 (2019)
- [91] Yang, H., Müller, W.H.: Size effects of mechanical metamaterials: A computational study based on a second order asymptotic homogenization method. *Arch. Appl. Mech.* (2020)
- [92] Yang, H., Timofeev, D., Giorgio, I., Müller, W.H.: Effective strain gradient continuum model of metamaterials and size effects analysis. *Contin. Mech. Thermodyn.* 1–23 (2020)
- [93] Yang, Y., Ching, W.Y., Misra, A.: Higher-order continuum theory applied to fracture simulation of nano-scale intergranular glassy film. *Journal of Nanomechanics and Micromechanics* 1(2), 60–71 (2011)
- [94] Yildizdag, M.E., Barchiesi, E., dell'Isola, F.: Three-point bending test of pantographic blocks: Numerical and experimental investigation. *Math. Mech. Solids* 1081286520916911 (2020)
- [95] Zervos, A., Papanicolopoulos, S.A., Vardoulakis, I.: Two finite-element discretizations for gradient elasticity. *Journal of Engineering Mechanics* 135(3), 203–213 (2009)

**How to cite this article:** Yang, H., Timofeev, D., Abali, B.E., Li, B., Müller, W.H. Verification of strain gradient elasticity computation by analytical solutions. *Z Angew Math Mech.* 2021;101:e202100023.  
<https://doi.org/10.1002/zamm.202100023>

## APPENDIX

### A.1 | The weak form and its numerical implementation

According to Equations (4), (5), (16), and (17), the weak form is shown as

$$\int_{\Omega} (\sigma_{ij} \delta u_{i,j} + \tau_{ijk} \delta u_{i,jk}) dV = \int_{\Omega} b_i \delta u_i dV + \int_{\partial\Omega} t_i \delta u_i dA + \int_{\partial\Omega} r_i D(\delta u_i) dA + \sum_m \oint_{\partial\partial\Omega_m} f_i \delta u_i dl, \quad (\text{A.1})$$

where  $r_i D(\delta u_i)$  is equal to  $r_i n_j \frac{\partial \delta u_i}{\partial X_j}$ , and  $n_j$  is the unit surface normal vector. For example, the  $n_j$  of the right surface in Figure 1(b) is equal to  $\delta_{1j}$ .

In this work, the wedge forces are constants and uniformly distributed on each edge with the unit of N/m. The total force acting on each edge is equal to  $f_i l$  in N.  $l$  in m is equal to the length of the corresponding edge. For example, in Section 4.2, the wedge forces on edge 2 is  $f_1$ . The total force acting on edge 2 is  $f_1 l$ . Instead of implementing the wedge forces directly, a traction with the amplitude of  $\frac{f_1}{2l_m}$  in Pa is applied on a small region (area of the region is  $2l_m l$ ) near edge 2 as shown in Figure A.1.

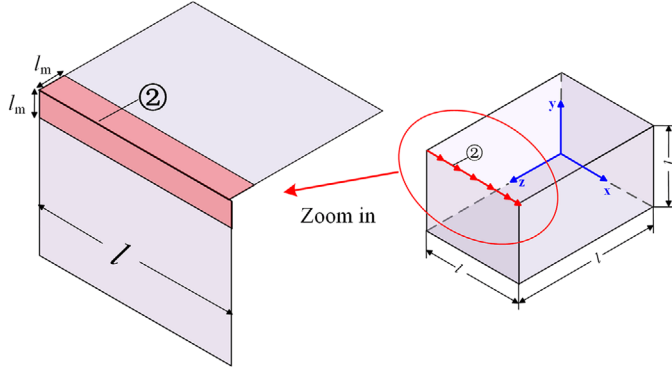


FIGURE A.1 The implementation of a wedge force on edge 2

For a detailed introduction of IGA we refer to [46]. In tIGAr, a self-contained implementation of single-patch explicit B-splines is realized by using a module called tIGAr.BSplines [50]. In this work, polynomial degree of the basis function has been chosen as 2 in order to acquire  $C^1$ -continuity for the formulation [39,81].

## A.2 | The derivation of Equation (6)

The derivation of Equation (6) is shown here. Equation (6) reads

$$\int_{\Omega} \left( \frac{\partial w}{\partial u_{i,j}} \delta u_{i,j} + \frac{\partial w}{\partial u_{i,jk}} \delta u_{i,jk} \right) dV = \int_{\Omega} \left( -\frac{\partial w}{\partial u_{i,j}} + \left( \frac{\partial w}{\partial u_{i,jk}} \right)_{,k} \right)_{,j} \delta u_i dV + \int_{\partial\Omega} n_j \left( \frac{\partial w}{\partial u_{i,j}} - \left( \frac{\partial w}{\partial u_{i,jk}} \right)_{,k} \right) \delta u_i dA + \int_{\partial\Omega} n_k \frac{\partial w}{\partial u_{i,jk}} \delta u_{i,j} dA. \quad (\text{A.2})$$

By using the divergence theorem, we can show that

$$\int_{\Omega} \left( \frac{\partial w}{\partial u_{i,j}} \delta u_i \right)_{,j} dV = \int_{\partial\Omega} n_j \left( \frac{\partial w}{\partial u_{i,j}} \delta u_i \right) dA. \quad (\text{A.3})$$

With the help of the product rule we have

$$\int_{\Omega} \left( \frac{\partial w}{\partial u_{i,j}} \delta u_i \right)_{,j} dV = \int_{\Omega} \left( \frac{\partial w}{\partial u_{i,j}} \right)_{,j} \delta u_i dV + \int_{\Omega} \frac{\partial w}{\partial u_{i,j}} \delta u_{i,j} dV. \quad (\text{A.4})$$

Therefore, the first term in the left hand side in in Equation (6) is rewritten as

$$\int_{\Omega} \frac{\partial w}{\partial u_{i,j}} \delta u_{i,j} dV = - \int_{\Omega} \left( \frac{\partial w}{\partial u_{i,j}} \right)_{,j} \delta u_i dV + \int_{\partial\Omega} n_j \left( \frac{\partial w}{\partial u_{i,j}} \delta u_i \right) dA. \quad (\text{A.5})$$

Likewise, from the divergence theorem, we can show that

$$\int_{\Omega} \left( \frac{\partial w}{\partial u_{i,jk}} \delta u_{i,j} \right)_{,k} dV = \int_{\partial\Omega} n_k \left( \frac{\partial w}{\partial u_{i,jk}} \delta u_{i,j} \right) dA. \quad (\text{A.6})$$

By using the product rule, we have

$$\int_{\Omega} \left( \frac{\partial w}{\partial u_{i,jk}} \delta u_{i,j} \right)_{,k} dV = \int_{\Omega} \left( \frac{\partial w}{\partial u_{i,jk}} \right)_{,k} \delta u_{i,j} dV + \int_{\Omega} \left( \frac{\partial w}{\partial u_{i,jk}} \right) \delta u_{i,jk} dV. \quad (A.7)$$

Therefore, the second term in the left hand side in Equation (6) is rewritten as

$$\int_{\Omega} \left( \frac{\partial w}{\partial u_{i,jk}} \right) \delta u_{i,jk} dV = \int_{\partial\Omega} n_k \left( \frac{\partial w}{\partial u_{i,jk}} \delta u_{i,j} \right) dA - \int_{\Omega} \left( \frac{\partial w}{\partial u_{i,jk}} \right)_{,k} \delta u_{i,j} dV \quad (A.8)$$

By using the divergence theorem and the product rule again,

$$\int_{\Omega} \left( \left( \frac{\partial w}{\partial u_{i,jk}} \right)_{,k} \delta u_i \right)_{,j} dV = \int_{\partial\Omega} n_j \left( \left( \frac{\partial w}{\partial u_{i,jk}} \right)_{,k} \delta u_i \right) dA, \quad (A.9)$$

$$\int_{\Omega} \left( \left( \frac{\partial w}{\partial u_{i,jk}} \right)_{,k} \delta u_i \right)_{,j} dV = \int_{\Omega} \left( \left( \frac{\partial w}{\partial u_{i,jk}} \right)_{,k} \right)_{,j} \delta u_i dV + \int_{\Omega} \left( \frac{\partial w}{\partial u_{i,jk}} \right)_{,k} \delta u_{i,j} dV. \quad (A.10)$$

Therefore,

$$\int_{\Omega} \left( \frac{\partial w}{\partial u_{i,jk}} \right)_{,k} \delta u_{i,j} dV = \int_{\partial\Omega} n_j \left( \left( \frac{\partial w}{\partial u_{i,jk}} \right)_{,k} \delta u_i \right) dA - \int_{\Omega} \left( \left( \frac{\partial w}{\partial u_{i,jk}} \right)_{,k} \right)_{,j} \delta u_i dV. \quad (A.11)$$

Consequently,

$$\int_{\Omega} \left( \frac{\partial w}{\partial u_{i,jk}} \right) \delta u_{i,jk} dV = \int_{\partial\Omega} n_k \left( \frac{\partial w}{\partial u_{i,jk}} \delta u_{i,j} \right) dA - \int_{\partial\Omega} n_j \left( \left( \frac{\partial w}{\partial u_{i,jk}} \right)_{,k} \delta u_i \right) dA + \int_{\Omega} \left( \left( \frac{\partial w}{\partial u_{i,jk}} \right)_{,k} \right)_{,j} \delta u_i dV \quad (A.12)$$

Therefore, we have

$$\begin{aligned} \int_{\Omega} \left( \frac{\partial w}{\partial u_{i,j}} \delta u_{i,j} + \frac{\partial w}{\partial u_{i,jk}} \delta u_{i,jk} \right) dV &= \int_{\Omega} \left( -\frac{\partial w}{\partial u_{i,j}} + \left( \frac{\partial w}{\partial u_{i,jk}} \right)_{,k} \right)_{,j} \delta u_i dV \\ &+ \int_{\partial\Omega} n_j \left( \frac{\partial w}{\partial u_{i,j}} - \left( \frac{\partial w}{\partial u_{i,jk}} \right)_{,k} \right) \delta u_i dA + \int_{\partial\Omega} n_k \frac{\partial w}{\partial u_{i,jk}} \delta u_{i,j} dA. \end{aligned} \quad (A.13)$$

### A.3 | Components of stress, hyperstress, and balance equations

The expressions for stress component in terms of displacement is explicitly given by

$$\sigma_{11} = c_1(\varepsilon_{11} + \varepsilon_{22} + \varepsilon_{33}) + 2c_2\varepsilon_{11} = c_1(u_{1,1} + u_{2,2} + u_{3,3}) + 2c_2u_{1,1}, \quad (A.14)$$

and for hyperstress components

$$\begin{aligned} \tau_{111} &= c_3(4u_{1,11} + u_{1,22} + 3u_{2,12} + u_{1,33} + 3u_{3,13}) + c_4(u_{1,11} + u_{2,21} + u_{3,31}) \\ &+ c_5(4u_{1,11} + 2u_{1,22} + 2u_{2,12} + 2u_{1,33} + 2u_{3,13}) + 2c_6u_{1,11} + 4c_7u_{1,11}. \end{aligned} \quad (A.15)$$

The other components can be calculated in the same manner. Equation (19) together with Equations (23)–(24) gives us the system of partial differential equations. For example, the balance equation in  $X_1$  direction is

$$\begin{aligned}
 & (c_1 + 2c_2)u_{1,11} + (c_1 + c_2)(u_{2,21} + u_{3,31}) + c_2(u_{1,22} + u_{1,33}) = (3c_3 + c_4 + 4c_5 + 2c_6 + 2c_7) \\
 & \times (u_{1,1111} + u_{2,2111} + u_{3,3111} + u_{1,1122} + u_{2,2122} + u_{3,3122} + u_{1,1133} + u_{3,3133} + u_{2,2133}) \\
 & + (c_3 + 2c_7)(u_{1,1111} + 2u_{1,1122} + 2u_{1,1133} + u_{1,2222} + 2u_{1,2323} + u_{1,3333}) - b_1.
 \end{aligned} \tag{A.16}$$